



OPEN

SUBJECT AREAS:
INACTIVATED VACCINES
IMMUNOLOGICAL MEMORY
SYSTEMS ANALYSIS
TIME SERIESReceived
13 May 2013Accepted
8 July 2013Published
31 July 2013Correspondence and
requests for materials
should be addressed to
H.W. (Hulin_Wu@
urmc.rochester.edu) or
M.S.Z.
(Martin_Zand@urmc.
rochester.edu)* These authors
contributed equally to
this work.

High-Resolution Temporal Response Patterns to Influenza Vaccine Reveal a Distinct Human Plasma Cell Gene Signature

Alicia D. Henn^{1,2*}, Shuang Wu^{2,3,4*}, Xing Qiu^{2,3,4}, Melissa Ruda^{1,2}, Michael Stover^{2,3,4}, Hongmei Yang^{2,3,4}, Zhiping Liu^{2,3,4}, Stephen L. Welle^{2,5}, Jeanne Holden-Wiltse^{2,3,4}, Hulin Wu^{2,3,4} & Martin S. Zand^{1,2}¹Department of Medicine, Division of Nephrology, ²Center for Biodefense Immune Modeling, ³Department of Biostatistics and Computational Biology, ⁴Center for Integrative Bioinformatics and Experimental Mathematics, ⁵Functional Genomics Center, University of Rochester School of Medicine and Dentistry, Rochester, New York, USA.

To identify sources of inter-subject variation in vaccine responses, we performed high-frequency sampling of human peripheral blood cells post-vaccination, followed by a novel systems biology analysis. Functional principal component analysis was used to examine time varying B cell vaccine responses. In subjects vaccinated within the previous three years, 90% of transcriptome variation was explained by a single subject-specific mathematical pattern. Within individual vaccine response patterns, a common subset of 742 genes was strongly correlated with migrating plasma cells. Of these, 366 genes were associated with human plasmablasts differentiating *in vitro*. Additionally, subject-specific temporal transcriptome patterns in peripheral blood mononuclear cells identified migration of myeloid/dendritic cell lineage cells one day after vaccination. Upstream analyses of transcriptome changes suggested both shared and subject-specific transcription groups underlying larger patterns. With robust statistical methods, time-varying response characteristics of individual subjects were effectively captured along with a shared plasma cell gene signature.

Pandemic and seasonal influenza causes significant morbidity and mortality worldwide. A key strategy in preventing influenza infection is vaccination, which induces B cells to differentiate through several stages into plasmablasts and long-lived plasma cells. These cells produce protective antibodies (immunoglobulin) against hemagglutinin (HA) capsid proteins¹. The World Health Organization (WHO) defines effective influenza vaccine responses as 28-day post-vaccine antibody hemagglutinin inhibition assay (HAI) titer $\geq 1:40^2$. However, influenza vaccines produce highly variable B cell responses among individuals³, making it difficult to predict who will achieve protective antibody titers and when.

Advances in data-driven personalized medicine, as applied to vaccine immunobiology, require new statistical methods that are able to capture immune response features common across subjects (e.g. consensus gene expression patterns) and patient-specific patterns which differ between subjects. This is especially true in vaccine studies. For example, recent studies on transcriptome patterns in vaccine responses have used sparse sampling (i.e. microarray analysis of PBMC on days 0, 3, and 7), and analytic methods that do not involve time series analysis⁴⁻⁶. In this report, we describe a robust systems biology approach using functional principal component analysis to identify common and subject-specific time-varying gene signatures within the trivalent influenza vaccine (TIV) immune response.

In a memory response to influenza vaccination, resting memory B cells differentiate through proliferating plasmablast states to terminally differentiated non-proliferating plasma cells⁷. Migrating through peripheral blood to bone marrow and spleen, virus-specific antibody-secreting cells (ASC) appear 5–9 days post-vaccination⁸. Vaccine or influenza exposure induces memory B cells producing cross-reactive antibodies to similar influenza strains, termed heterosubtypic immunity⁹. The presence of heterosubtypic immunity alters the speed and strength of TIV responses. Previous systems biology vaccine response analyses have sampled subjects on a single day empirically described as the peak B cell response^{10,4}. Such approaches lack the structure to capture peak responses or the statistical power to separate time varying gene signatures from inter-subject variation. Our approach is fundamentally different. Our goal was instead to identify differences in the character of the tran-



scriptome responses of individuals using high-frequency sampling and an analytical method designed to characterize temporal patterns in complex systems. In contrast to other studies^{10,4}, we were not trying to predict who responded to the vaccine. Rather, our goal was a deeper understanding of the time varying, vaccine specific, transcriptome response, and to determine if the B and plasma cell gene expression patterns varied as a function of pre-existing vaccine antigen memory. Systems analysis of high-frequency time course data requires more samples per subject, but better defines peak and time varying B cell immune responses.

To separate consensus from subject-specific time-varying B cell transcriptome responses to influenza vaccination, we performed high-frequency (daily) sampling of serum, peripheral blood mononuclear cells (PBMC), B cells and plasma cells from 14 human subjects over 11 days post-TIV administration. Our approach combined time-series transcriptome analysis, flow cytometry, ELISPOT, ELISA, and HAI assays with computational analysis to identify time-varying RNA biomarkers associated with robust B cell responses. To identify subject-specific gene expression signatures, we used functional principal component analysis (FPCA), a statistical dimension reduction method for high frequency time series data similar to principal component analysis for single time-point data^{11,12}. In essence, the differential expression of each gene is determined by its own signal-to-noise ratio. The major temporal variation in the RNAseq time-series data can be characterized by a few representative patterns called eigenfunctions. Each gene expression curve is approximated by a linear combination of these eigenfunctions, enabling a flexible and parsimonious representation of time-series data. This method accommodated individuality in vaccine response by identifying time-varying transcriptome patterns unique to each subject. For a detailed explication of FPCA, and underlying statistical theory, please see the specific section in Supplementary Methods.

This approach identified a peripheral blood B cell transcriptome signature in previously vaccinated subjects that was strongly correlated with migrating plasma cells observed with cytometry. Upstream analysis of significant gene sets revealed common immunological dynamics between subjects as well as unique vaccine response features in individuals. At the subject level, these responses were associated with robust protective antibody responses and a prior history of influenza vaccination. Eigenfunctions calculated for PBMC gene expression also demonstrated an early wave of myeloid/dendritic cell lineage migration peaking 24 hours post-vaccination. Additional eigenfunctions identified transcriptome changes unique to each individual, commonalities between subject-specific signatures, and their relative contribution to the overall vaccine response.

Results

Heterogeneous antibody responses to TIV vaccination. We vaccinated three cohorts of 3–6 subjects ($n = 14$ subjects) with the 2010–2011 TIV. Subjects reported mixed vaccine histories, with two subjects reporting no influenza vaccination in three consecutive years prior to the study, and three subjects reporting receiving all available influenza vaccines. Two of study vaccine strains, A/California/7/2009 and B/Brisbane/60/2008 were included in recent vaccines (Supplementary Table S1).

For analysis, peripheral blood was drawn during the week prior to vaccination (pre-V), immediately before vaccination (day 0), daily for days 1–10 and on day 21 post-vaccination. HAI and isotype-specific ELISA assays were performed on serum samples. (Fig. 1, Supplementary Fig. S1). No two subjects had identical changes in HAI titers. One subject had no pre-vaccine immunity ($\text{HAI} < 1:40$), and five subjects had pre-vaccine immunity ($\text{HAI} \geq 1:40$) to all three viral strains (Fig. 1, Supplementary Table S2). At day 21, all 14 subjects had immunity to A/California, 12 had immunity to A/Perth and 13 had immunity to B/Brisbane.

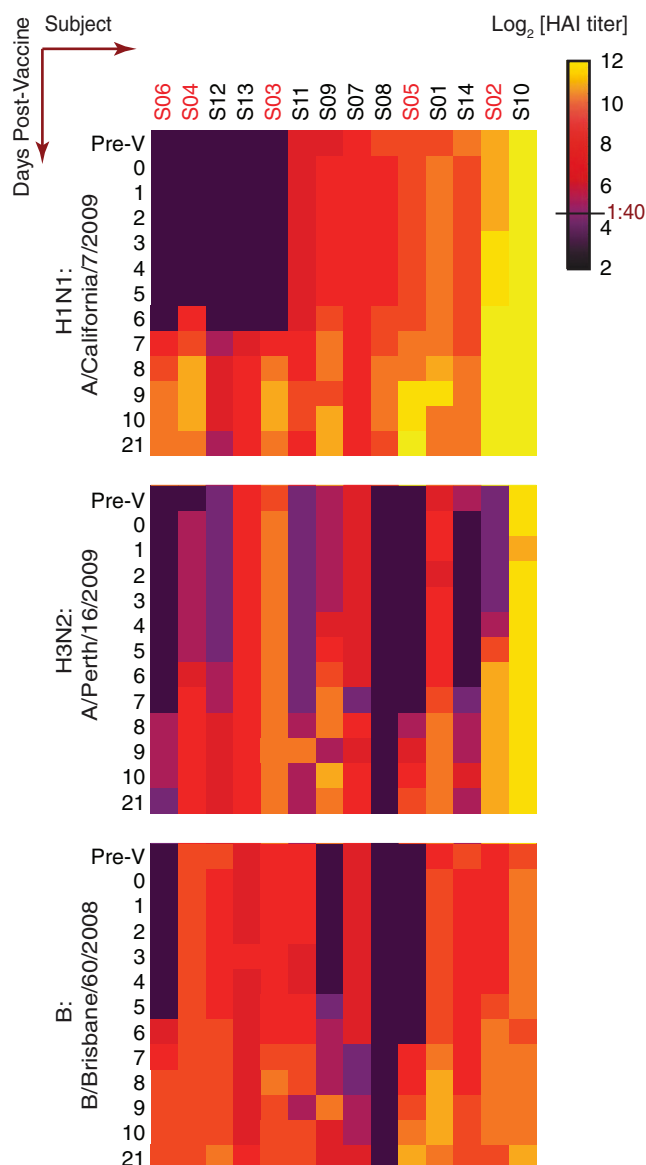


Figure 1 | Hemagglutinin Inhibition Activity of Daily Serum Samples. Blood was drawn one day within a week prior to vaccination (pre-V), at vaccination (day 0), daily days 1 to 10, and day 21 after vaccination. Serum samples showed heterogeneous humoral responses to the three virus types in the vaccine, A/California/7/2009 (A/California), A/Perth/16/2009 (A/Perth), and B/Brisbane/60/2008 (B/Brisbane). With immunity classified as an HAI titer $> 1:40$, S06 was not previously immune to any of the three viruses. S05, who had reported not being vaccinated in the previous three years, was immune to A/California only. S01, S07, and S10 were initially immune to all three viruses and the other subjects showed a mix of initial immunity. At day 21, all subjects except S08 and S12 qualified as immune. See also Supplementary Figure S1 and Supplementary Tables S1 and S2.

Differences in gene expression correlate with vaccine history and response. B cell samples (days 0–10) were analyzed by RNAseq, flow cytometric and ELISPOT (880 samples) (Supplementary Fig. S1). Due to cost, RNA Seq analysis was performed on PBMC and B cell enriched samples from one contemporaneous cohort of five subjects, days 0 to 10 (110 samples). S01 RNA was used for RNA Seq pilot studies. We selected a single cohort of subject samples for RNA Seq analysis. Each gene was tested for differential change from day 0 to day 10 using FPCA-based significance testing¹³ and a permutation test coupled with multiple-testing correction to control the false discovery rate ($\text{FDR} < 0.05$)¹⁴. A deviation in a gene expression



curve from a flat line indicates a significant temporal pattern in transcriptomic variation.

Intra-subject variation in differentially expressed genes was moderate (p-values in Supplementary Table S3). S02 had the largest number of significantly time-varying genes (5580 genes) while S06 had few (2 genes). For better comparison with other subjects, 1600 genes with the highest signal to noise ratio were added to the analysis of S06. After excluding genes with less than a 1.2-fold-change from baseline, the numbers of temporally differentially expressed genes still varied greatly: S02 (5256 genes), S03 (1309 genes), S04 (2147 genes), S05 (1603 genes) and S06 (1053 genes). Notably, 742 genes were common to three of five subjects.

We next used FPCA to identify the major variations in temporal RNA expression patterns of the differentially expressed genes for each subject, which were then represented by eigenfunctions (Fig. 2a, complete list of significantly time-varying genes in Supplementary Table S3). For three subjects (S02, S03, S04), 90% of transcriptome variation could be accounted for by a single eigenfunction. All three of these subjects had a previous history of influenza vaccination, pre-vaccine immunity to at least one viral vaccine strain by WHO criteria, and strong antibody responses by HAI titer (Fig. 2b, p-values in Supplementary Table S2) and vaccine-specific ELISA (Fig. 2c, p-values in Supplementary Table S2).

Cellular responses were seen by FACS in the appearance of vaccine-specific ASC (Fig. 2d), and migrating $CD27^{hi}CD38^{hi}CD20^{lo}CD138^{+}$ plasma cells and $CD27^{hi}CD38^{hi}CD20^{lo}CD138^{-}$ plasmablasts (Fig. 2e, p-values in Supplementary Table S4). In semi-quantitative ELISPOT data, (Supplementary Fig. S2), we found secretion-rate profiles typical of activated ASC¹⁵, with high-rate vaccine-specific IgG-secreting cells appearing at peak responses.

Subject-specific dynamics were seen in vaccine response characteristics at multiple levels. S02 had a sharp peak in cellular and RNA changes at day 5, whereas S03 and S04 had more gradual changes. These subjects met serum and cellular criteria for robust memory B cell responses to TIV. However, with some evidence of *de novo* reactivity to A/California, and without specific clone data, we prefer the term “predominantly recall” responses.

In two subjects (S05, S06), 90% of the variation in gene expression could be explained by two eigenfunctions, indicating two distinct temporal patterns of gene expression. S06 had a linear trend in some genes and S05 had multimodal eigenfunctions. These subjects reported no influenza vaccination in the previous three years and developed *de novo* immunity to at least two vaccine-specific viruses by WHO HAI criteria. Acknowledging the difficulties in defining an influenza response in adults as truly naive, we prefer the term “predominantly *de novo*” responses.

Taken together, results from the high frequency sampling data show coordinated and dynamic vaccine-response changes at serum, cellular, and transcriptomic levels, as well as inter-subject variations in immunological response characteristics. Features of time-varying transcriptome profiles independently identified subjects with significant pre-vaccine B cell memory. Also, high-frequency sampling provided the resolution to discern unique expression dynamics across assays for each subject.

Transcriptome changes in the B cell predominantly recall response were consistent with late B cell differentiation. To connect the transcriptomic and cellular level B cell influenza vaccine responses, we hypothesized that predominantly recall TIV responses would be characterized by significant variations in established markers of late B cell differentiation (Fig. 2f). Detailed analysis showed known genes with time-varying patterns that paralleled B cell phenotypic changes in S02, S03 and S04 including the genes for CD70 receptor $CD27^{16-18}$, ecto-enzyme $CD38^{16}$, plasma cell marker syndecan-1 (SDC1 or CD138), and genes encoding regulatory molecules PRDM1 (Blimp-1)^{19,7}, IRF4^{16,20,21} and XBP1²². Also increased was *CD59*, which has

been associated with memory B cell differentiation²³. Increased expression of *CXCR3*, a gene for a migration marker²⁴ suggested trafficking from the germinal center through peripheral blood presumably to bone marrow and spleen. Decreases in *MS4A1* (CD20) and *CD19* at peak cellular changes are also consistent with late-stage differentiating B cells^{16,25,26,23}. *PAX5*⁷ and *BACH2*²⁷ are known repressors of B cell differentiation and decreased gene expression has been linked to expression of *PRDM1*²⁸. In subjects with predominantly *de novo* responses (S05, S06) time-varying expression of these differentiation markers was modest or absent.

Decreases were seen at peak response in *CD5*, the gene expressing a marker of naïve B cells, and *SERPINB9* (PI-9), an enzyme that protects cytolytic B cells from endogenously produced granzyme B²⁹. It has been proposed that a granzyme B expressing cytolytic B cell lineage diverges from plasmablasts during differentiation³⁰. Reduced expression of these markers may reflect ASC fractional expansion post-vaccination.

To confirm and validate changes in expression of key B cell differentiation genes, we probed RNA samples of the eight other subjects by qRT-PCR for 11 genes: *SDC1*, *IGHG*, *XBP1*, *CD27*, *CD38*, *CD59*, *PRDM1*, *IRF4*, *IRF8*, *BACH2*, and *PAX5*. These subjects were heterogeneous in vaccine response by HAI titer (Fig. 3a), vaccine-specific ELISA (Fig. 3b), and flow cytometry (Fig. 3c). Changes in migrating B cells and plasma cells over time exhibited a similar pattern in these independent subjects (Fig. 3d and Supplementary Table S5).

A strong gene expression signature post-TIV in previously vaccinated subjects is associated with migrating plasma cells.

In comparing significant time-varying gene sets between individuals, we found a biomarker signature of 742 genes common to predominantly recall subjects (Fig. 4, p-values in Supplementary Table S6). To identify statistically significant connections between transcriptomic and cellular levels, we compared phenotypic and gene expression data using Pearson’s correlation test with the Benjamini-Hochberg multiple test correction to control FDR at 0.05. Out of 742 genes shared among the previously vaccinated individuals, 740 (S02), 404 (S03), and 238 (S04) genes were significantly correlated with $CD27^{hi}CD38^{hi}CD138^{-}$ plasmablasts, indicating a very strong association. This gene set was even more highly correlated with $CD27^{hi}CD38^{hi}CD138^{hi}$ plasma cells. Out of 742 shared genes, 742 (S02), 553 (S03), and 725 (S04), were correlated with plasma cells (FDR < 0.05) (Fig. 5a, correlations in Supplementary Table S6). These associations were strong in all three subjects, even though the timing of peak expression, and composition of genes within the broader significant gene sets, varied between subjects. We refer to this set of 742 genes as the plasma cell gene signature (PCgs).

Expression of the PCgs in late-stage differentiating B cells subsets.

We next asked if the PCgs could be validated by examining transcriptome data from *in vitro* human plasma cell differentiation. Peripheral blood $CD27^{+}$ IgG⁺ memory B cells from six normal healthy volunteers were CFSE labeled to track proliferation and stimulated *in vitro* for 60 hrs with CpG₂₀₀₆ ODN, IL-2, IL-10, IL-15, and BAF²³. For transcriptome analysis, cells were FACS-sorted into three stages of late-stage memory B cell activation and differentiation; undivided $CD27^{lo}$ memory B cell, proliferating $CD27^{lo}$ cells and proliferating $CD27^{hi}$ plasmablasts (Fig. 5b) (n = 6 subjects). We hypothesized that a subset of PCgs genes would be differentially expressed between the $CD27^{lo}$ (proliferating but non-IgG secreting) B cell and the more differentiated $CD27^{hi}$ plasmablasts (Fig. 5c). Of 2033 genes differentially expressed between $CD27^{lo}$ and $CD27^{hi}$ B cells, 366 genes of the PCgs were highly expressed in the $CD27^{hi}$ plasmablasts (Fig. 5d, full gene list in Supplementary Table S6). These independent findings strengthen the association between the PCgs and differentiating plasma cell subtypes (Fig. 5e).

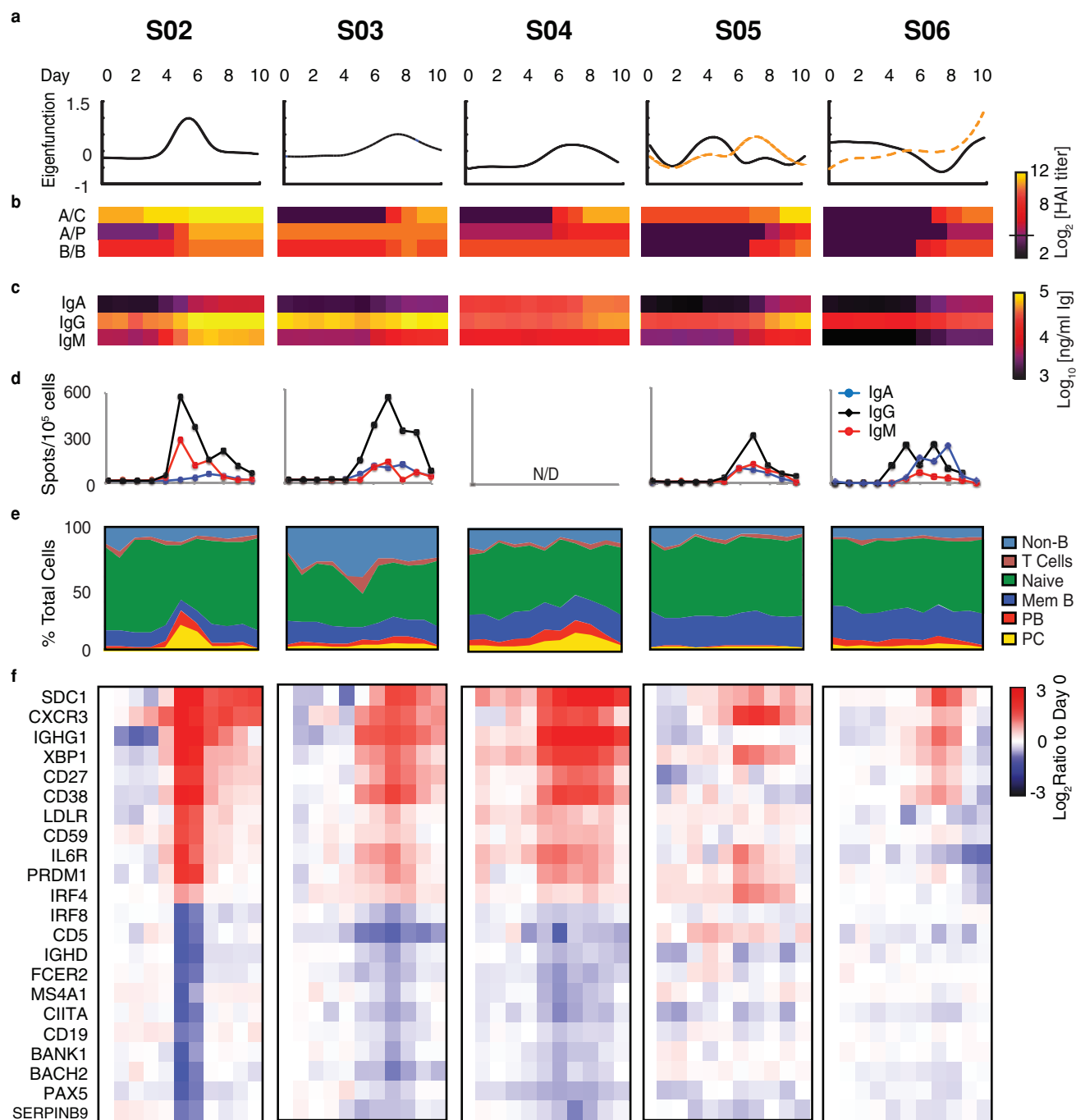


Figure 2 | Subject-specific B cell vaccine response characteristics. (a) A single gene expression eigenfunction accounted for 90% of sample variation in each subject vaccinated in the previous three years (S02, S03, and S04). Multiple eigenfunctions were found in RNA Seq data of subjects not previously vaccinated (S05, S06) (full list of significant genes in Supplementary Table S3). (b) By HAI titer, S02, S03 and S04 had previous immunity to two HA antigens. S02 had increases in antibody levels at least 24 hours before S03 and S04 (p-values, Supplementary Table S2). (c) Anti-vaccine IgM, IgG, and IgA levels parallel changes in HAI titer (p-values Supplementary Table S2). (d) ELISPOT assays show functional vaccine-specific IgA, IgG, and IgM ASC increase as serum antibody levels increase. (e) Phenotypic changes of $\text{CD}3^- \text{CD}19^+ \text{CD}20^+ \text{CD}27^-$ naive B cells, $\text{CD}19^+ \text{CD}27^+ \text{CD}20^+ \text{CD}38^+ \text{CD}138^-$ memory B cells, $\text{CD}19^+ \text{CD}27^{++} \text{CD}38^{++} \text{CD}138^-$ plasmablasts and $\text{CD}19^+ \text{CD}20^+ \text{CD}27^{++} \text{CD}38^{++} \text{CD}138^+$ plasma cells. Plasmablast and plasma cell populations increase as ASC appear (p-values Supplementary Table S4). (f) Expression of genes (ratio to day 0) change as expected based on available literature in S02, S03 and, S04 (p-values, Table S3). *CD5* and *SERPINB9* levels decrease at peak response consistent with a fractional decrease in naive and cytolytic B cells. Fewer genes changed significantly in S06 and S05, subjects reporting no vaccination in the previous 3 years. S02 showed peak response at day 5, earlier than S03 and S04. (N/D = no data).

Common upstream regulatory mechanisms in the PCGs. Given the strength of the *in vivo* and *in vitro* associations between the plasma cell population kinetics and the PCGs at the gene level, it seemed likely that there were common upstream regulatory transcription

factors. We performed upstream analysis on gene expression data from S02 using Ingenuity® Pathways Analysis (IPA). Fisher's exact test was used to assess overlap between the data set and curated gene sets associated in the literature with upstream modulators

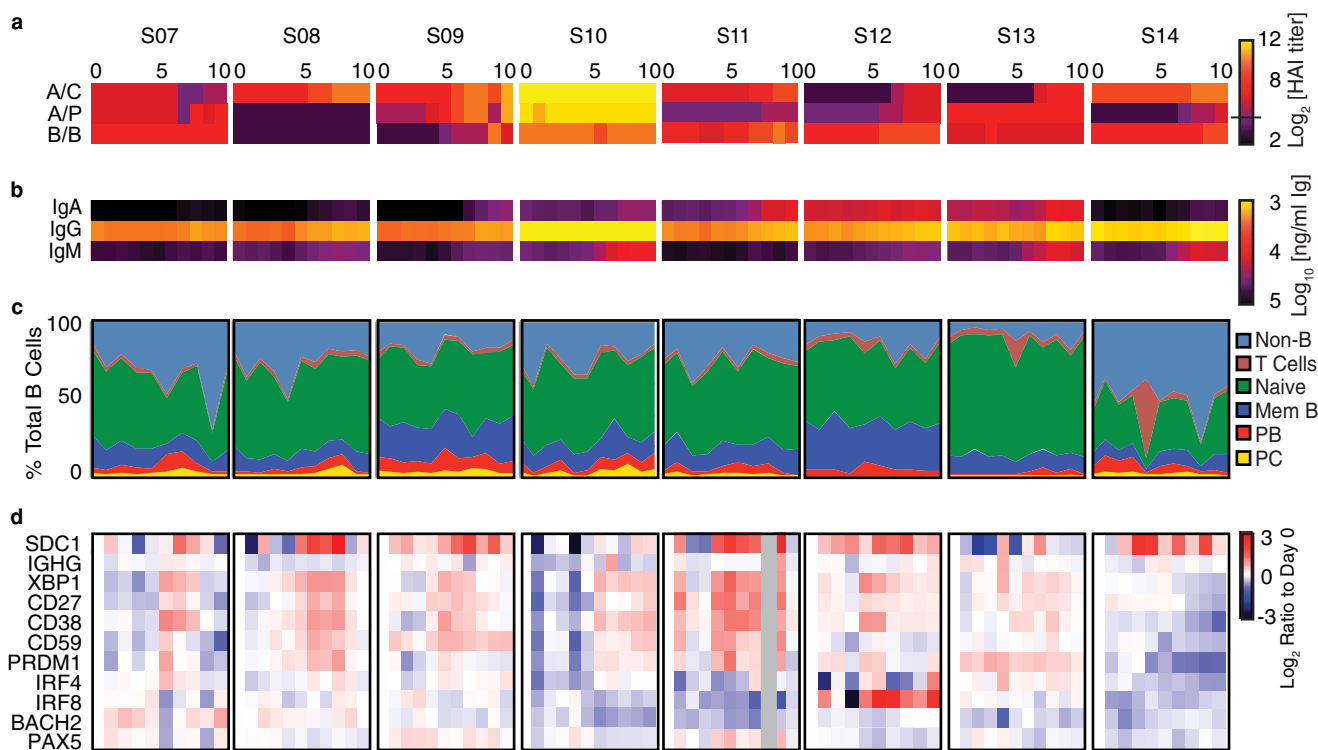


Figure 3 | Quantitative RT-PCR confirms patterns of expression of B cell Differentiation Genes. To confirm expression levels of B cell differentiation genes by qRT-PCR, we assayed RNA from eight subjects collected in two cohorts previous to the cohort used for RNA Seq data. These subjects had varied serum vaccine responses as assessed by (a) HAI titer, (b) vaccine-specific ELISA, and (c) flow cytometric analysis. Expansion of plasmablasts and plasma cell numbers were not clear in all subjects. T cell contamination was evident in two samples. (d) Increased expression of CD27, CD38, XBP1, CD59, PRDM1 and IRF4 and decreased expression of IRF8, BACH2, and PAX5 was expected at peak plasmablast/plasma cell expansion. While not all genes correlated with phenotype (correlations in Supplementary Table S5), expression levels changed as expected based on phenotype.

(www.ingenuity.com). We constructed a time series movie of a network of identified upstream modulators (p -value < 0.01) and their targets, (see Supplementary Movie S1). Gene expression changes consistent with release of suppression of B cell regulator *PRDM1* (Blimp1) by *BACH2*²⁷ occur by day 4. In days 4 through 10, upregulation of *XBP1* was seen, as well as downstream genes associated with ER function, the unfolded protein response, protein production and transport. We also performed functional enrichment analyses of Gene Ontology (GO) terms using DAVID (<http://david.abcc.ncifcrf.gov/>) and analyses of pathways with KEGG, BIOCARTA and REACTOME (Supplementary Table S7). Ten of the top 30 categories of functionally related genes in the PCgs involved ER function and protein production. These findings are consistent with involvement of the PCgs in program-level upregulation of antibody production machinery and the unfolded protein response seen during plasma cell development²⁸.

Unique as well as shared B cell response features beneath the larger patterns. In addition to the common PCgs, each subject had unique time-varying gene sets. We hypothesized that these may reflect differences between subjects in regulatory transcription factors. Using the complete set of significant genes for each predominantly recall subject, upstream analysis identified a likely set of upstream activators (Z -score > 2.0) that spanned the peak B cell response in all three subjects (Fig. 6). IL2, IL4, IL5, IL6 and CD40 ligand were identified as probable activators. While the signaling pathways of these activators are not mutually exclusive, this is consistent with a plasma cell history of germinal center reaction.

In addition to common upstream activators, each subject also had a unique set of significantly varying transcription factors. Of particular interest, a wave of probable activation of Type I IFN and

IFN-related gene sets appeared in S04 two days after the shared germinal center pattern. This could be evidence of a secondary migration of B cells with previous plasmacytoid dendritic cell (pDC) interaction within the broader peak response. Producers of large amounts of Type I Interferons, pDC are part of the innate response to virus and can induce antibody production by CD40-stimulated B cells in response to influenza^{31,32}. As interferon regulatory factor (IRF) proteins can also regulate B cell differentiation in response to toll-like receptor stimulation^{33,34}, another interpretation of this pattern is a viral DNA-initiated innate response to the vaccine. The eigenfunctions derived by the analysis, along with upstream analysis, identified both common and subject-specific dynamic gene sets that may represent the effects of interacting innate and adaptive cellular immune systems on differentiating plasma cell.

Myeloid cell gene signatures peak in PBMC primary eigenfunctions at Day 1. We next hypothesized that the PCgs could be identified in PBMC collected in parallel with the B cell samples. We found something quite unexpected. The primary eigenfunction in the RNA Seq gene expression data, which explained over 70% of the variation for four out of five subjects (S02, 81.44%; S03, 86.68%; S04, 72.8%; S05, 57.15%; S06, 85.32%), peaked on day 1 post-vaccination (Fig. 7a). In the predominantly recall subjects, the genes with largest positive loadings on the primary eigenfunction were enriched for myeloid/dendritic cell (DC) lineage-associated genes (Fig. 7b, Supplementary Table S8). Interestingly, the first eigenfunctions for predominantly de novo response subject S06 also contained myeloid/DC genes with more modest overall gene expression changes. These results suggest that even within the far more complex and dynamic mix of cellular populations in post-vaccination PBMC, FPCA analysis could identify a wave of

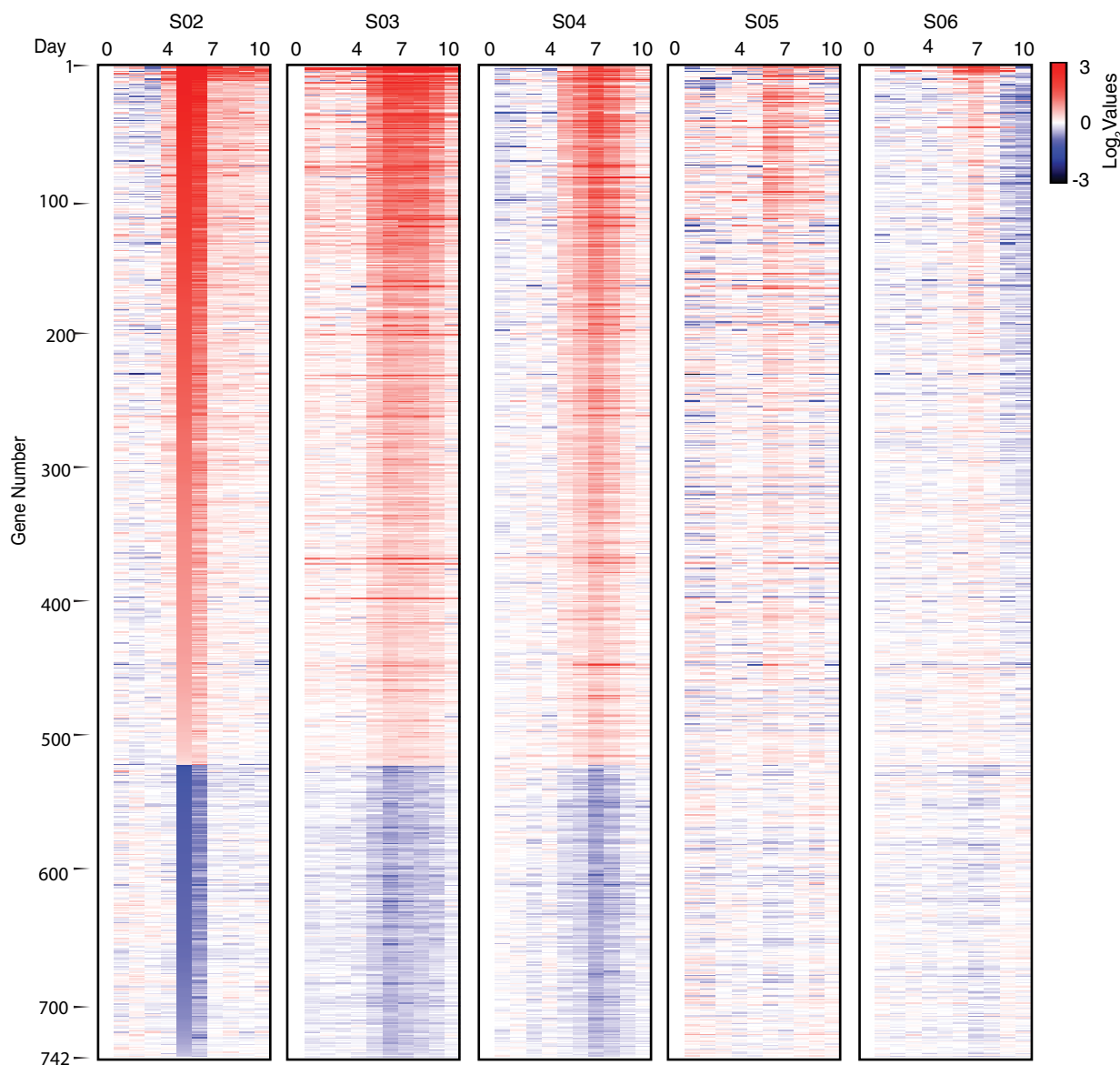


Figure 4 | A common set of 742 significant genes in subjects that had been previously vaccinated. Day 0 normalized gene expression values for the common set of 742 significant genes in S02, S03, and S04. These subjects reported influenza vaccination within the past three years (Red indicates increased gene expression level, blue indicates decreased levels). S02, which had the earliest peak response, had received all available influenza vaccines in the previous 3 years. Samples from S05 and S06, who reported no vaccination in the previous three years, had fewer significantly time-varying genes (S05, 174 genes) (S06, 2 genes) in common with the others (p-values in Supplementary Table S6).

myeloid lineage cells released into peripheral blood one day post-influenza vaccination in four of five subjects.

Discussion

Using a method based on FPCA for time-series transcriptome analysis, we identified a 742 gene signature, upstream transcription factors, and subject-specific gene sets associated with a robust B cell response to influenza vaccine. The method yields quantitative functions (eigenfunctions) that describe the temporal pattern of major transcriptome variation. In previously vaccinated subjects, the 742 gene signature was highly correlated with the migration of differentiating plasma cells through peripheral blood. There was an association between the PCgs and key upstream transcription factors that control antibody production including *PRDM1* and *XBP1*. A second gene signature was identified in unfractionated PBMC with a transcriptome profile suggesting migration of cells of the myeloid/DC lineage one day post-vaccination. In addition to these common

gene signatures, eigenfunctions identified specific points of variation between individuals including a late spike in IFN-related gene activity. Thus, this approach can identify processes common across individuals in a vaccine response, as well as unique features that may underlie variation between subjects.

A systems biology approach to studies of B cell response requires not only connections between nested levels of regulation from genes to the whole organism, but also perturbations in these systems over time. This study was designed to capture frequent and complete B cell gene expression dynamics after influenza vaccination in a small set of subjects. In this study, high-frequency data from each subject serves as an intra-subject control, adding statistical power and accuracy for detection of significant signals from noisy transcriptome data. A better understanding of vaccine-induced subject-specific gene dynamics may help design studies with more subjects and fewer timepoints that still capture transcriptome patterns.

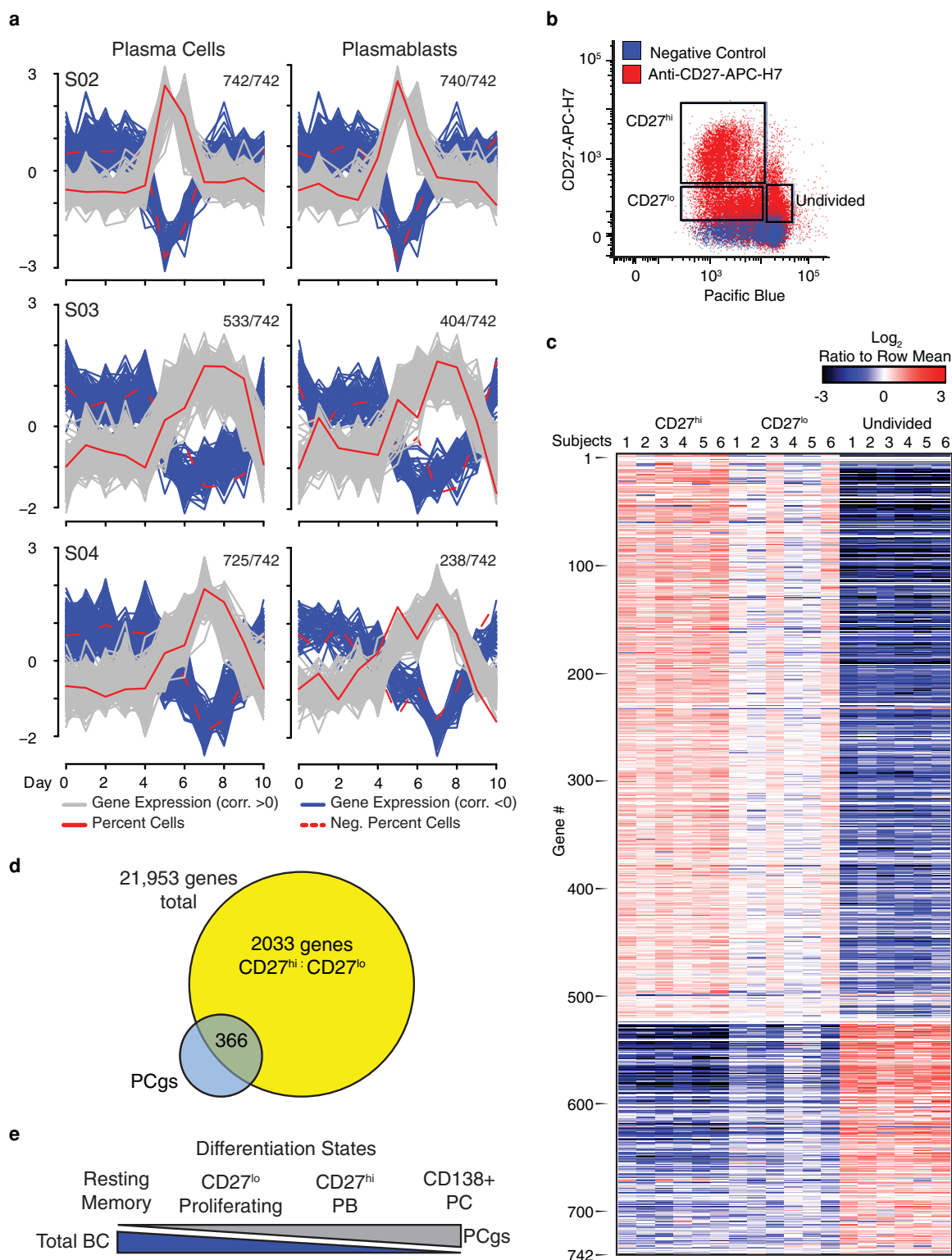


Figure 5 | Expression of the PCgs in Differentiating Plasma Cells. (a) We found strong correlations between PCgs expression and CD19⁺ CD27⁺⁺ CD38⁺⁺ CD138⁻ plasmablasts and CD19^{lo}CD20^{lo}CD27⁺⁺ CD38⁺⁺ CD138⁺ plasma cell percentages (number of correlating genes in each panel). (b) Normal human IgM⁻ B cells were stained with pacific blue succinimidyl ester (PBSE) to show proliferation and stimulated for 60 hr in vitro with CpG2009 ODN and cytokines IL-2, IL-10, IL-15, and BAFF (n = 6 subjects). The cells were FACS-sorted into three stages of differentiation (Undivided, CD27^{lo}, and CD27^{hi}). (c) Row-normalized RNA expression levels from gene array data previously published by our group²³ were re-examined for the PCgs (genes ordered as Figure 4 and Supplementary Table S6, red = upregulation, blue = downregulation). Genes upregulated in the PCgs also tended to be upregulated in the most differentiated CD27^{hi} cells, expressed at moderate levels in less differentiated CD27^{lo} cells, and at lowest levels in undivided cells. The converse was true of PCgs downregulated genes. (d) Of 2033 genes significantly different between CD27^{lo} and the more differentiated CD27^{hi} plasmablasts, 366 genes were shared with the PCgs (full list, Supplementary Table S6). (e) The proportion of PCgs genes expressed increased as resting memory B differentiated through plasmablast states and then to fully differentiated CD138⁺ plasma cells.

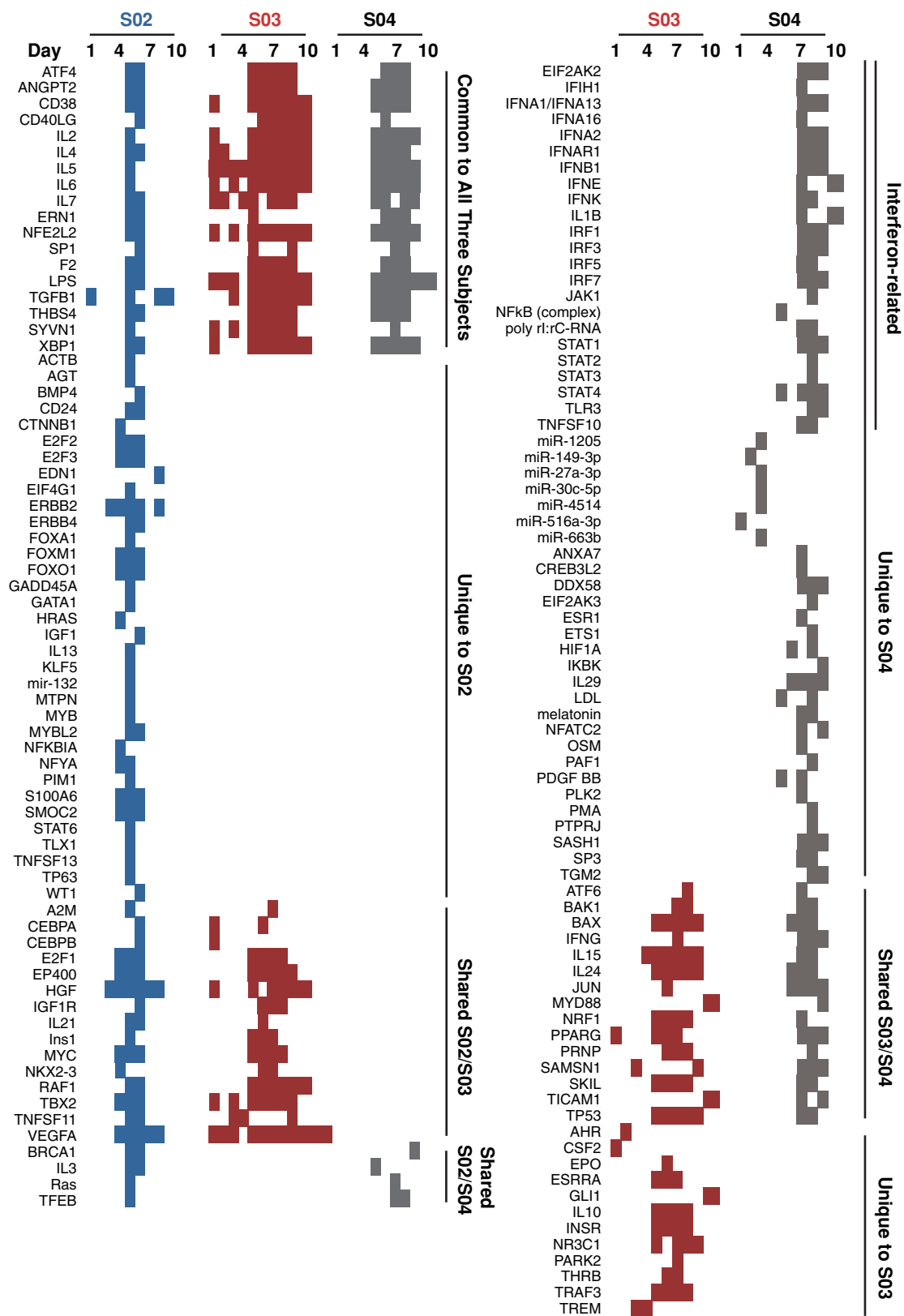


Figure 6 | Upstream analysis of time-varying B cell gene sets. Ingenuity Pathways Analysis of significant time-varying genes of subjects S02 (5256 genes), S03 (1309 genes), S04 (2147 genes) was performed. Upstream modifiers with a Z-score of 2.0 or higher, indicating probable activation, are shown. Molecule sets downstream of these modifiers were not mutually exclusive. All three subjects showed probable activation by upstream cytokines typical of the germinal center reaction, including IL2, IL4, IL5, IL6 and CD40LG across days of peak response. Upstream modifiers unique to each subject suggested immunological differences. Of interest, late in the peak response of S04, IFN-related signaling molecules were identified. This could be the result of a previous innate-type stimulus such as interaction with plasmacytoid dendritic cells or viral DNA-initiated toll-like receptor activation. Our method identified dynamic gene regulation patterns with common as well as subject-specific upstream regulatory elements underlying the larger post-vaccine response.

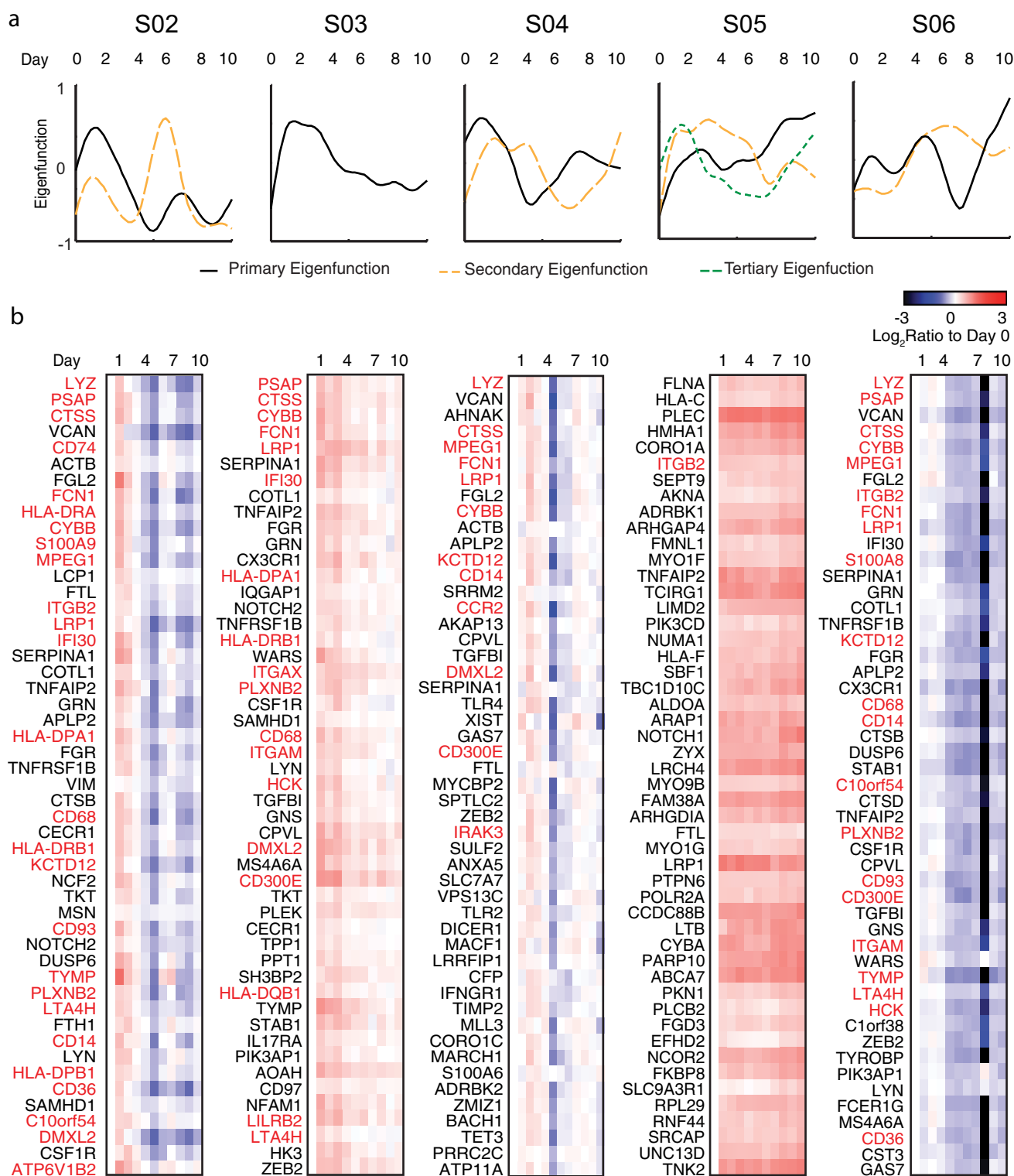


Figure 7 | PBMC Gene Expression Patterns Suggest Myeloid/Dendritic Cell Migration. PBMC were isolated in parallel with enriched B cell samples. (a) FPCA analysis of RNA Seq data showed a primary eigenfunction that explained over 70% of the variation across the timepoints for four subjects (S02, 81.44%) (S03, 86.68%) (S04, 72.8%) (S05, 57.15%) (S06, 85.32%). Second eigenfunctions explained most of the remaining variation in three subjects (S02, 13.11%) (S03, 7.24%) (S06, 10.2%). S05 had a third eigenfunction that explained 13.85% of variation. The first eigenfunction for S02, S03, and S04 peaked day 1. (b) The largest positive loadings on these functions were enriched for genes expressed by myeloid/DC lineages (gene symbols in red), (Supplementary Table S8). The first eigenfunction for S05 had few myeloid/DC genes. Second and third eigenfunctions, peaking day 1, both contained small numbers of myeloid/DC genes. The first eigenfunction of S06 peaking on day 1 was enriched for myeloid/DC genes, but expression changes were modest. Day 8 there was a sample processing error.



The use of eigenfunctions to identify common patterns of gene expression that explain transcriptome variations is a powerful analytic method. Inter-subject vaccine response heterogeneity is considerable^{3,9,4}. To generalize conclusions, other systems biological studies have averaged gene expression data across subjects¹⁰ or restricted their analyses to significant genes shared in at least 20% of subjects⁴. Our goal was not to predict vaccine efficacy in large groups of people and indeed, all of our subjects achieved protective HAI titers. Our goal was to identify differences between the vaccine responses of individual subjects over time, and to identify dynamic gene expression mechanisms that underlie those differences. Our method approached subject variation by identifying subject-specific time-varying transcriptome signatures and *within those unique patterns*, identifying a B cell response gene set shared among individuals. This approach may yield more robust insights into immune response dynamics than sampling at wide time intervals (e.g. only days 0, 4 and 7 post-vaccination), which misses critical events in the individual response. While other studies have found plasma cell associated genes upregulated on Day 7^{6,4}, we found subject-specific variation in peak expression of PCGs that would have been missed with typical interval sampling.

Using high-frequency sampling, we found that subjects that had been previously vaccinated each had individual response characteristics, but 90% of the gene expression variation over time could be accounted for by a single subject-specific eigenfunction containing a common plasma cell transcriptome signature. This gene signature was identical in all three of the previously vaccinated subjects. As our sample size is small and all of our subjects for RNA Seq achieved protective HAI titers for the vaccine antigens, it is difficult to compare vaccine efficacy with incidence of the PCGs. One interpretation suggested by our findings is that the predominantly recall influenza vaccine responses exhibited a synchrony of B cell differentiation across vaccine-specific memory B cell populations, while the predominantly *de novo* responses did not. In combination with stochastic nature of plasma cell fate determination³⁵, this synchrony of initiation likely resulted in a wave of differentiating plasma cell migrating from the germinal center of individuals with B cell memory.

PBMC eigenfunctions contained a signature suggesting migration of myeloid/DC lineage cells 24 hours after vaccination. Our results are quite consistent with a recent study using transcriptional analysis of whole blood after influenza vaccination⁵. In this study, neutrophils and monocytes were implicated as the major source of the IFN-related gene set upregulated within 15 hours post-vaccination for influenza. Interferon-related transcripts upregulated one day after Influenza vaccination in an earlier study were also correlated with anti-Influenza antibody titers⁶. This myeloid/DC gene signature likely triggers the initial germinal center reaction that results in plasma cell migrations later.

At the organ level in normal human subjects, we cannot sample lymph nodes and spleen. However, our analysis suggests that with higher temporal transcriptome resolution, peripheral blood does reveal evidence of prior upstream gene regulation, reflecting hidden dynamic events within lymphoid compartments. Also, upstream transcriptome analysis revealed that migration of multiple B cell populations underlie broader B cell and plasma cell surface marker phenotypes observed by flow cytometry. Further detailed experiments are needed to determine if transcriptome patterns observed are from broad changes in B cell population cell frequencies or a single dominating subpopulation. Given that our PBMC analysis reflects mixed and dynamic cell populations, any resulting gene interaction network cannot be considered strictly causal, but rather should be interpreted as a network of temporally associated transcriptome changes, likely occurring in several cell populations. Further and more detailed cell sorting work will need to be done to validate this hypothesis.

At the cellular level, division-linked B cell differentiation^{36,37,38} is asymmetric with key control molecules like BCL-6 bequeathed to one daughter cell³⁹. This, along with graded *IRF4* expression²¹, is thought to affect diversification of B cells. Our findings suggest that even with diverse B cell fates, a common transcriptomic signature can identify pre-existing vaccine-specific B cell memory, likely a marker for heterosubtypic immunity. During a pandemic, the PCGs may be useful in early prediction of both successful vaccine responses and heterosubtypic immunity.

At the individual gene level, within the PCGs we identified key plasma cell regulatory genes including those seen in other systems biology studies. *TNFRSF17*¹⁰ was found in both *in vitro* and *in vivo* data sets, and *XBPI*^{4,40} was central to our networks. Our high-frequency sampling extends these observations with detailed time-series data capturing individual response patterns. Other genes previously associated with the post-vaccination neutralizing antibody response include *KBTBD7*¹⁰, which did not significantly change. We also found more genes specifically associated with plasma cells than previous studies. Whether this difference is due to the statistical strength of high-frequency sampling and FPCA, or other methodological differences, will be addressed in future studies.

Finally, we would like to note that FPCA-based time-series transcriptome analysis extends beyond simple statistical analysis. The method of FPCA and the form of the results are well suited for application to machine learning in computational modeling⁴¹. In replacing instinctive or heuristic approaches with a rigorous mathematical method that can approximate behaviors of a complex biological system, FPCA lends itself to the utilization of artificial intelligence methods in models and systems biology analyses. Specifically, the resulting eigenfunctions and matrix formulations allow more rigorous characterization and modeling of complex cellular and transcriptome responses.

In conclusion, these data provide evidence for a novel transcriptomic signature associated with differentiating B cell and plasma cell migration through peripheral blood B cell pools in subjects previously vaccinated for influenza. They also suggest that with further study, temporal transcriptome patterns that accommodate individual variation may illuminate more detailed system dynamics underlying large-scale responses. The method of FPCA may also allow robust modeling and systems analysis of immune responses using artificial intelligence and machine learning methods.

Methods

Human subjects protection. This study was approved by the Research Subjects Review Board at the University of Rochester Medical Center. Informed consent was obtained from all participants. Research data were coded such that subjects could not be identified, directly or through linked identifiers, in compliance with the Department of Health and Human Services Regulations for the Protection of Human Subjects (45 CFR 46.101(b)(4)). Subject identification numbers were re-encoded for publication.

Myeloma cell culture. Myeloma cell lines were maintained in log-phase growth as previously described⁴² and used for controls in flow cytometry and ELISPOT assays: MPR-1130 (established in our laboratory), MC/CAR, Ramos cell lines (ATCC, Manassas, VA), NCI-H929 (ATCC, Manassas, VA).

Peripheral blood mononuclear cell (PBMC) isolation. Each daily blood sample for each subject was pooled from heparinized blood collection tubes and a portion removed for PBMC analysis. Lymphocytes were isolated using discontinuous Ficoll gradient centrifugation from buffy coat samples. Magnetic anti-CD235 immunoaffinity beads (Miltenyi Biotec, Auburn, CA) were used to remove RBC contaminants.

B cell isolation. B cell samples were enriched from heparinized whole blood with RosetteSep Immunodensity separation (Stemcell Technologies, Vancouver, BC, Canada). Negative magnetic immunoaffinity bead separation columns (Miltenyi Biotec, Auburn, CA) were used with anti-CD3 (BD Bioscience, San Diego, CA) and anti-CD235 beads (Miltenyi Biotec, Auburn, CA) to further purify total B cells. Flow cytometric analysis was performed on all isolates, showing >90% purity of the isolates.



Flow cytometric assay. Data was collected as previously described⁴³ with FACS Diva data acquisition software on an LSR II cytometer. Analysis of data utilized Flowjo software (Treestar, Ashland, OR). Antibodies used included anti-CD138-APC, anti-CD20-V450 (BD Bioscience, San Diego, CA), anti-CD19-PE-Texas Red, anti-CD27-PE-Cy5, (Beckman Coulter, Indianapolis, IN), anti-CD38-PE-Cy7 (eBioscience, San Diego, CA), anti-CD3-PECy5.5 (Southern Biotech, Birmingham, AL), anti-B7-FITC (Santa Cruz Biotechnology, Santa Cruz, CA), anti-CCR10-PE (Biolegend, San Diego, CA), anti-CD62L-APC-Alexa-750, and Live/Dead Aqua (Invitrogen, Grand Island, NY).

Flow cytometry analysis. Before analysis with Flow clustering without K (FLOCK) software (<https://import.niaid.nih.gov>), compensation and initial gating to remove debris and dead cells was completed using FlowJo (TreeStar). Files for each subject were then concatenated, uploaded to ImmPort and analyzed using FLOCK 1.0⁴⁴ to identify centroids for representative clusters across the timepoints. The following markers were used: CD19, CD20, CD138, CD3, CD27, CD38, B7, CCR10 and CD62L. Individual timepoint sample files were then analyzed against the centroids file, assigning all events to a cluster, using the Cross Sample Comparison feature of Flock. A semi supervised clustering method was used to cluster centroids to identify non-B cells (CD19⁻, CD3⁻), T cells (CD19⁻, CD3⁺), naive B cells (CD19⁺, CD3⁻, CD20⁺, CD27⁻), memory B cells (CD19⁺, CD3⁻, CD20⁺, CD27⁺), plasmablasts (CD19⁺, CD3⁻, CD20⁻, CD138⁻) and plasma cells (CD19⁺, CD3⁻, CD20⁻, CD138⁺). Percentages of each phenotype were calculated for each sample.

Hemagglutinin inhibition analysis (HAI). Hemagglutinin assays were performed as previously described⁴⁵ using the 2012–2011 WHO Influenza reagent Kit for identification of influenza isolates (WHO Collaborating Center for Surveillance, Epidemiology and Control of Influenza) and the Seiken method to remove non-specific inhibitors of hemagglutination.

RNA Seq. RNA was extracted with the Qiagen RNeasy micro kit. Concentrations were determined by UV spectrophotometry (Nanodrop) and integrity of ribosomal RNA was confirmed with the Agilent Bioanalyzer. Barcoded sequencing libraries were prepared with Illumina TruSeq RNA kits as recommended by Illumina, using 100 ng total RNA as input. All samples from an individual subject were sequenced in the same run using an Illumina Genome Analyzer Ix (22 samples per 8 lanes). CASAVA programs (Illumina, version 1.7) were used to demultiplex samples according to barcode, align sequences with the genome, and count how many sequences aligned with known variants of RefSeq genes (data are not separated according to splice variants). Sequences (reads) per gene per million total RefSeq reads were computed, with no adjustment for transcript length.

Quantitative RT-PCR. Immediately after collection, peripheral blood cell isolates were lysed in RLT buffer, passed through a Qias shredder column (Qiagen, Germantown, MD) and snap frozen in liquid nitrogen. Samples were stored at -70°C until RNA extraction, performed using the RNeasy Micro Kit with on-column DNase (Qiagen). Quantitative RT-PCR was performed on three experimental replicates per sample in TaqMan[®] Array Fast Plates with TaqMan[®] Universal PCR Master Mix, No AmpErase[®] UNG on the StepOnePlus[™] Real-Time PCR System (Life Technologies, Carlsbad, CA) with 10 ng cDNA into each 10 μl reaction. RNA quality was confirmed by the presence of intact rRNA with an Agilent 2100 Bioanalyzer (Santa Clara, CA). For analysis, relative quantity (RQ) values for each gene were calculated using $\Delta\Delta\text{CT}$ (Cq) method⁴⁶. Cq values for each gene were normalized to the mean Cq from a group of six reference genes (ACTB, POLR2A, MTA2, THRAP3, USP4, CERS2) that were chosen empirically because they were unaffected by vaccination in all five subjects from whom RNAseq data were available.

Semi-quantitative ELISpot estimation of IgG secretion. Photocleavable antibody-coated paramagnetic beads were prepared as previously published²³. B cell isolates were plated in ELISPOT plates coated as indicated below and incubated at 37°C for 5 hours. The plates were washed and plates for IgG and IgA detection were soaked overnight in PBS + 0.1% Tween20. Plates for IgM detection were stored at 4°C overnight in PBS before a 1 hr soak. At each time point, ELISPOT plates were developed as previously published using Alkaline Phosphate Substrate Kit III (Vector Laboratories, Burlingame CA)¹⁵. ELISPOT well membranes were removed from plates and scanned on an HP Scanjet 8300 high-resolution scanner and well images analyzed using ELIScan and EXPLORAspot custom software as previously published⁴⁷.

Reagents for ELISPOT and ELISA. Wells of 96-well ELISPOT and ELISA plates were coated with 3.2 mcg/ml 2010–2011 trivalent influenza vaccine for assay of TIV-specific antibody secretion for virus-specific reactivity, or 4 $\mu\text{g}/\text{ml}$ goat-anti-human IgM + IgA + IgG (KPL, Gaithersburg, MD) for total IgA, IgG, or IgM. Detection reagents for separate isotype-specific assays included goat anti-human IgM, goat anti-human IgG, and goat anti-human IgA reagents that were phosphatase-labeled for ELISPOT (KPL, Gaithersburg, MD) or peroxidase-labeled for ELISA (KPL, Gaithersburg, MD). ELISA assays were developed using 1-Step Ultra TMB substrate (Pierce Biotechnology, Rockford, IL).

Statistical methods. *Functional principal component analysis.* Significance testing of the time-series RNA Seq data was performed using Eigen-bases estimated from Functional Principal Component Analysis as published in Wu et al¹³, and a test

statistic of the goodness of fit of the model. The multiple test correction method proposed by Benjamini and Hochberg¹⁴ was followed to control the false discovery rate (FDR).

Upstream analysis. Data sets containing RNA Seq gene expression values were uploaded into Ingenuity Pathways Analysis (IPA) (<http://ingenuity.com/>). Each identifier was mapped to its corresponding object in Ingenuity's Knowledge Base. Network eligible molecules were overlaid onto a global molecular network developed from information contained in Ingenuity's Knowledge Base. Networks of Network Eligible Molecules were then algorithmically generated based on their connectivity. A series of network figures with overlaid daily gene expression data was made using Upstream Analysis in IPA, Adobe Illustrator and Acrobat Professional CS5 (Adobe, San Jose, CA). Upstream analysis modulator Z-scores of 2 and above were considered probable activators (-2 for inhibitors).

Functional gene enrichment analysis. We performed the standard GO functional enrichment analysis using DAVID (<http://david.abcc.ncifcrf.gov/>). The reported p-values were derived from the EASE score probability 'p-Value', and a modified Fisher's exact test that is more conservative than the standard Fisher's exact test. Benjamini-Hochberg correction was used. 'BIOCARTA', 'KEGG_PATHWAY', and 'REACTOME_PATHWAY' were used for pathway enrichment analysis of these clusters. We set the DAVID EASE threshold to default and ranked the enriched functions and pathways for each cluster.

Microarray gene expression analysis. Previously published *in vitro* microarray gene expression data²³ from CpG-stimulated normal IgM- human B cells were examined for the 742 gene PCGs seen in our *in vivo* data. Where multiple probe sets corresponded to one gene, we reported the single probe set with the highest interquartile range.

Correlations of RNA Seq and qRT-PCR data with cell phenotypes. Pearson's test for pair-wise correlation was used to test each gene and the percentage of each cellular phenotype. The Benjamini-Hochberg procedure¹⁴ was used to control FDR at 0.05 level.

Significance testing of phenotypic changes and serum antibody changes. For the significance test of changes in the percent of cells by phenotype and antibody levels, we used a variant of the EDGE method⁴⁸ without multiple testing correction. For the day of 50% increase, we used a method similar to Zaslavsky et al⁴⁹.

1. Waffarn, E. E. & Baumgarth, N. Protective B cell responses to flu-no fluke! *J Immunol* **186**, 3823–3829 (2011).
2. Eichelberger, M. *et al.* FDA/NIH/WHO public workshop on immune correlates of protection against influenza A viruses in support of pandemic vaccine development, Bethesda, Maryland, US, December 10–11, 2007. *Vaccine* **26**, 4299–4303 (2008).
3. Wang, M. L., Skehel, J. J. & Wiley, D. C. Comparative analyses of the specificities of anti-influenza hemagglutinin antibodies in human sera. *J. Virol.* **57**, 124–128 (1986).
4. Nakaya, H. I. *et al.* Systems biology of vaccination for seasonal influenza in humans. *Nat Immunol* **12**, 786–795 (2011).
5. Bucacas, K. L. *et al.* Early patterns of gene expression correlate with the humoral immune response to influenza vaccination in humans. *J. Infect. Dis.* **203**, 921–929 (2011).
6. Obermoser, G. *et al.* Systems scale interactive exploration reveals quantitative and qualitative differences in response to influenza and pneumococcal vaccines. *Immunity* **38**, 831–844 (2013).
7. Oracki, S. A., Walker, J. A., Hibbs, M. L., Corcoran, L. M. & Tarlinton, D. M. Plasma cell development and survival. *Immunol. Rev.* **237**, 140–159 (2010).
8. Kyu, S. Y. *et al.* Frequencies of human influenza-specific antibody secreting cells or plasmablasts post vaccination from fresh and frozen peripheral blood mononuclear cells. *J. Immunol. Methods* **340**, 42–47 (2009).
9. Corti, D. *et al.* Heterosubtypic neutralizing antibodies are produced by individuals immunized with a seasonal influenza vaccine. *J. Clin. Invest.* **120**, 1663–1673 (2010).
10. Querec, T. D. *et al.* Systems biology approach predicts immunogenicity of the yellow fever vaccine in humans. *Nat Immunol* **10**, 116–125 (2009).
11. Yao, F., Müller, H. G. & Wang, J.-L. Functional data analysis for sparse longitudinal data. *J Am Stat Assoc* **100**, 577–590 (2005).
12. Ramsay, J. O. & Silverman, B. W. Functional data analysis 2nd edition. *Springer Series in Statistics* (2005).
13. Wu, S. & Wu, H. More Powerful Significant Testing for Time Course Gene Expression Data Using Functional Principal Component Analysis Approaches. *BMC Bioinformatics* **14** (2013).
14. Benjamini, Y. & Hochberg, Y. Controlling the False Discovery Rate - a Practical and Powerful Approach to Multiple Testing. *Journal of the Royal Statistical Society Series B-Methodological* **57**, 289–300 (1995).
15. Henn, A. D. *et al.* Modulation of single-cell IgG secretion frequency and rates in human memory B cells by CpG DNA, CD40L, IL-21, and cell division. *J. Immunol.* **183**, 3177–3187 (2009).



16. Tarte, K., Zhan, F., De Vos, J., Klein, B. & Shaughnessy, J., Jr. Gene expression profiling of plasma cells and plasmablasts: toward a better understanding of the late stages of B-cell differentiation. *Blood* **102**, 592–600 (2003).
17. Klein, U. *et al.* Transcriptional analysis of the B cell germinal center reaction. *Proc. Natl. Acad. Sci. U. S. A.* **100**, 2639–2644 (2003).
18. Avery, D. T. *et al.* Increased expression of CD27 on activated human memory B cells correlates with their commitment to the plasma cell lineage. *J. Immunol.* **174**, 4034–4042 (2005).
19. Radbruch, A. *et al.* Competence and competition: the challenge of becoming a long-lived plasma cell. *Nature reviews. Immunology* **6**, 741–750 (2006).
20. Klein, U. *et al.* Transcription factor IRF4 controls plasma cell differentiation and class-switch recombination. *Nat Immunol* **7**, 773–782 (2006).
21. Sciammas, R. *et al.* Graded expression of interferon regulatory factor-4 coordinates isotype switching with plasma cell differentiation. *Immunity* **25**, 225–236 (2006).
22. Reimold, A. M. *et al.* Transcription factor B cell lineage-specific activator protein regulates the gene for human X-box binding protein 1. *J. Exp. Med.* **183**, 393–401 (1996).
23. Henn, A. D. *et al.* Functionally Distinct Subpopulations of CpG-Activated Memory B Cells. *Sci Rep* **2**, 345 (2012).
24. Trentin, L. *et al.* The chemokine receptor CXCR3 is expressed on malignant B cells and mediates chemotaxis. *J. Clin. Invest.* **104**, 115–121 (1999).
25. Kuo, T. C. *et al.* Repression of BCL-6 is required for the formation of human memory B cells in vitro. *J. Exp. Med.* **204**, 819–830 (2007).
26. Jourdan, M. *et al.* An in vitro model of differentiation of memory B cells into plasmablasts and plasma cells including detailed phenotypic and molecular characterization. *Blood* **114**, 5173–5181 (2009).
27. Ochiai, K. *et al.* Plasmacytic transcription factor Blimp-1 is repressed by Bach2 in B cells. *J. Biol. Chem.* **281**, 38226–38234 (2006).
28. Shaffer, A. L. *et al.* XBP1, downstream of Blimp-1, expands the secretory apparatus and other organelles, and increases protein synthesis in plasma cell differentiation. *Immunity* **21**, 81–93 (2004).
29. Hirst, C. E. *et al.* The intracellular granzyme B inhibitor, proteinase inhibitor 9, is up-regulated during accessory cell maturation and effector cell degranulation, and its overexpression enhances CTL potency. *J. Immunol.* **170**, 805–815 (2003).
30. Hagn, M. *et al.* Human B cells differentiate into granzyme B-secreting cytotoxic B lymphocytes upon incomplete T-cell help. *Immunol. Cell Biol.* **90**, 457–467 (2012).
31. Cella, M. *et al.* Plasmacytoid monocytes migrate to inflamed lymph nodes and produce large amounts of type I interferon. *Nat. Med.* **5**, 919–923 (1999).
32. Jego, G. *et al.* Plasmacytoid dendritic cells induce plasma cell differentiation through type I interferon and interleukin 6. *Immunity* **19**, 225–234 (2003).
33. Doyle, S. *et al.* IRF3 mediates a TLR3/TLR4-specific antiviral gene program. *Immunity* **17**, 251–263 (2002).
34. Takaoka, A. *et al.* Integral role of IRF-5 in the gene induction programme activated by Toll-like receptors. *Nature* **434**, 243–249 (2005).
35. Duffy, K. R. *et al.* Activation-induced B cell fates are selected by intracellular stochastic competition. *Science* **335**, 338–341 (2012).
36. Hodgkin, P. D., Lee, J. H. & Lyons, A. B. B cell differentiation and isotype switching is related to division cycle number. *J. Exp. Med.* **184**, 277–281 (1996).
37. Deenick, E. K., Gett, A. V. & Hodgkin, P. D. Stochastic model of T cell proliferation: a calculus revealing IL-2 regulation of precursor frequencies, cell cycle time, and survival. *J. Immunol.* **170**, 4963–4972 (2003).
38. Hasbold, J., Corcoran, L. M., Tarlinton, D. M., Tangye, S. G. & Hodgkin, P. D. Evidence from the generation of immunoglobulin G-secreting cells that stochastic mechanisms regulate lymphocyte differentiation. *Nat Immunol* **5**, 55–63 (2004).
39. Barnett, B. E. *et al.* Asymmetric B cell division in the germinal center reaction. *Science* **335**, 342–344 (2012).
40. Gaucher, D. *et al.* Yellow fever vaccine induces integrated multilineage and polyfunctional immune responses. *J. Exp. Med.* **205**, 3119–3131 (2008).
41. Glickman, M., Balthrop, J. & Forrest, S. A machine learning evaluation of an artificial immune system. *Evol. Comput.* **13**, 179–212 (2005).
42. Zand, M. S. *et al.* Apoptosis and complement-mediated lysis of myeloma cells by polyclonal rabbit antithymocyte globulin. *Blood* **107**, 2895–2903 (2006).
43. Huggins, J. *et al.* CpG DNA activation and plasma-cell differentiation of CD27-naive human B cells. *Blood* **109**, 1611–1619 (2007).
44. Qian, Y. *et al.* Elucidation of seventeen human peripheral blood B-cell subsets and quantification of the tetanus response using a density-based method for the automated identification of cell populations in multidimensional flow cytometry data. *Cytometry. Part B, Clinical cytometry* **78 Suppl 1**, S69–82 (2010).
45. Kobie, J. J. *et al.* Decreased influenza-specific B cell responses in rheumatoid arthritis patients treated with anti-tumor necrosis factor. *Arthritis Res Ther* **13**, R209 (2011).
46. Livak, K. J. & Schmittgen, T. D. Analysis of relative gene expression data using real-time quantitative PCR and the 2^{(-Delta Delta C(T))} Method. *Methods* **25**, 402–408 (2001).
47. Rebhahn, J. A. *et al.* Automated analysis of two- and three-color fluorescent Elispot (Fluorospot) assays for cytokine secretion. *Comput. Methods Programs Biomed.* **92**, 54–65 (2008).
48. Storey, J. D., Xiao, W., Leek, J. T., Tompkins, R. G. & Davis, R. W. Significance analysis of time course microarray experiments. *Proc Natl Acad Sci U S A* **102**, 12837–12842 (2005).
49. Zaslavsky, E. *et al.* Antiviral response dictated by choreographed cascade of transcription factors. *J Immunol* **184**, 2908–2917 (2010).

Acknowledgements

We would like to thank Tim Mosmann, David Topham, Mark Sangster, Tim Bushnell, Danielle C. Alc na, Shannon Hilchey, and the members of the University of Rochester Center for Biodefense Immune Modeling for spirited discussions that greatly improved the manuscript. We would like to thank study nurse Margaret McGrath as well as Yanfang Huang, Sarah Alef, Danielle Morsch, Michelle Zanche and the URMIC genomics core, and the URMIC Flow Core for their expert technical assistance. This work was supported by NIH grant number HHSN272201000055C (A.D.H., M.S.Z., S.L.W., J.H.-W., M.R., M.S., S.W., X.Q., Z.L., H.W.), R01 AI098112 and R01 AI069351 (M.Z., M.R., A.D.H.).

Author contributions

M.S.Z. and H.W. conceived the study. A.D.H., M.S.Z. and H.W. designed the experiments. A.D.H. performed the experiments and transcriptomic analysis and S.L.W. performed the FPCA analysis. H.W. supervised the data analysis. S.W., X.Q., M.S., H.Y., Z.L. and J.H.-W. performed the statistical analysis of the data, Z.L. performed GSEA analysis, M.R. performed FLOCK analysis of flow cytometric data, S.L.W. supervised the RNA data collection and pre-analysis/processing. A.D.H., M.S.Z., S.L.W., S.W., X.Q. and H.W. wrote the manuscript.

Additional information

Supplementary information accompanies this paper at <http://www.nature.com/scientificreports>

Competing financial interests: The authors declare no competing financial interests.

How to cite this article: Henn, A.D. *et al.* High-Resolution Temporal Response Patterns to Influenza Vaccine Reveal a Distinct Human Plasma Cell Gene Signature. *Sci. Rep.* **3**, 2327; DOI:10.1038/srep02327 (2013).



This work is licensed under a Creative Commons Attribution-NonCommercial-NoDerivs 3.0 Unported license. To view a copy of this license, visit <http://creativecommons.org/licenses/by-nc-nd/3.0>